Scanning probe microscopy based on magnetoresistive sensing

2011 Nanotechnology 22 145501

(http://iopscience.iop.org/0957-4484/22/14/145501)

Nanotechnology **22** (2011) 145501 (8pp) doi:10.1088/0957-4484/22/14/145501

Scanning probe microscopy based on magnetoresistive sensing

Deepak R Sahoo[1], **Abu Sebastian, Walter Häberle, Haralampos Pozidis and Evangelos Eleftheriou**

IBM Research—Zurich, Säumerstrasse 4, 8803 Rüschlikon, Switzerland

E-mail: hap@zurich.ibm.com

Received 30 December 2010, in final form 5 January 2011
Published 24 February 2011
Online at stacks.iop.org/Nano/22/145501

Abstract
Integrated sensors are essential for scanning probe microscopy (SPM) based systems that employ arrays of microcantilevers for high throughput. Common integrated sensors, such as piezoresistive, piezoelectric, capacitive and thermoelectric sensors, suffer from low bandwidth and/or low resolution. In this paper, a novel magnetoresistive-sensor-based scanning probe microscopy (MR-SPM) technique is presented. The principle of MR-SPM is first demonstrated using experiments with magnetic cantilevers and commercial MR sensors. A new cantilever design tailored to MR-SPM is then presented and micromagnetic simulations are employed to evaluate the achievable resolution. A remarkable resolution of 0.84 Å over a bandwidth of 1 MHz is estimated, which would significantly outperform state-of-the-art optical deflection sensors. Due to its combination of high resolution at high bandwidth, and its amenability to integration in probe arrays, MR-SPM holds great promise for low-cost, high-throughput SPM.

(Some figures in this article are in colour only in the electronic version)

1. Introduction

Scanning probe microscopy (SPM) based devices have numerous potential practical applications, such as bio-sensing, maskless lithography, semiconductor metrology and ultrahigh-density data storage [1–6]. However, despite their truly great potential, stemming from their ability to interrogate and manipulate matter at the nanometer-scale, SPM devices still mainly remain niche laboratory instruments, mostly because of their limited speed of operation and their small 'field-of-view', typically on the order of tens of micrometers. To achieve high throughput and large field-of-view, these devices typically employ multiple probes in parallel operation [7–11]. Current moderate-speed SPM setups typically use an optical deflection sensing system with a position-sensitive photodetector (PSD) for moderate bandwidth and high resolution imaging [12–15]. However, these conventional optical detection systems are too bulky and expensive for parallel probe high-throughput devices. To develop such devices at reasonable footprint and cost, the deflection sensor needs to be integrated onto the microcantilever during the fabrication process.

There are several ways to extend optical beam deflection sensing to an array of probes. One such method employs sequential detection using a scanning laser and an array of photodiodes [16, 17]. In a similar approach, the laser beam is focused on the entire area of the array of probes and the deflected beams are captured through a charge coupled device (CCD) camera and tracked in real time by an image processing (centroid-based) algorithm to detect the probes simultaneously [18]. In another approach, the optical interferometric detection technique is extended to an array of probes by fabricating the probes with interdigitated fingers, and by using a cylindrical laser (to illuminate the entire array of probes) and an array of photodiodes [19]. The fiber-optic-based interferometric technique can be integrated on probes by fabricating a Bragg grating as a photo-elastic strain sensor [20]. Optical sensing can also be integrated on probes that are fabricated as (total internal reflection) waveguides and butt-coupled at the free end to another waveguide to sense the deflection as a change in the optical intensity of the transmitted light [21–26]. However, such in-plane photonic transduction techniques cannot easily be extended to a large array of probes because they use a complex network of waveguides and/or an array of photodiodes. In general, optical deflection sensing

[1] Present address: H H Wills Physics Laboratory, University of Bristol, Tyndall Avenue, Bristol BS8 1TL, UK.

with a laser and an array of photodiodes may achieve high bandwidth and high resolution, but remains an expensive and bulky way to sense an array of probes. Moreover, none of the aforementioned methods is scalable to large probe arrays, thus their usage is limited to some niche applications.

In contrast to multi-probe optical detection, which relies on elements external to the probe for sensing, a variety of other sensors exist that can be integrated on the probe during the fabrication process. Piezoresistive [27] and piezoelectric [28] elements can be deposited on the probe as strain sensors to detect the deflection of the micro-structure. However, deposition of such materials results in high stiffness and generates unwanted stress in the probe structure. Moreover, the inherent noise in such strain sensors limits the resolution for nano-scale imaging [29]. MEMS comb structures can be fabricated on the probes as capacitors, and the probes can be detected in parallel in an integrated manner [10, 30]. Such a design requires highly sensitive electronics to detect very small currents (in the picoampere range). Moreover, parasitic capacitances inevitably limit the resolution and bandwidth of sensing. Thermoelectric sensors can easily be integrated on probes by fabricating micro-heater regions with differential doping. Such sensors can provide high resolution when used appropriately, i.e., with an efficient heat conduction path to the sample. However, the bandwidth of sensing is limited to a few tens of kHz, owing to the limited bandwidth of the thermal system [31].

In this paper, a novel cantilever displacement sensing technique using magnetoresistive (MR) sensing is presented. MR spin-valve sensors have already been used in scanning magnetoresistance microscopy by fabricating a MR structure on the back side of the cantilever [32, 33]. These cantilevers were used to image the magnetic field variation on the surface of a sample. In contrast, in our work, the MR sensors are used to sense the cantilever displacement signal for generic SPM applications. The essential idea is to translate the cantilever displacement into a change in the magnetic field as sensed by the MR sensor. This mode of scanning probe microscopy is henceforth referred to as MR-SPM. It promises nano-scale resolution and high bandwidths in excess of 1 MHz for high-speed SPM. Moreover, it is an integrable technique and thus scalable to large probe arrays for very high throughput. MR-SPM possesses all the necessary ingredients for building a new breed of multi-probe SPM devices that could find widespread use. As such, it has the potential to revolutionize scanning probe microscopy. An earlier version of this work, describing only the basic concept of MR-SPM and some preliminary experiments was presented in [34].

The remainder of the paper is arranged as follows. In section 2, the motivation behind using magnetoresistive sensors for SPM is presented. In section 3, a proof-of-concept experiment is presented to illustrate the concept of MR-SPM. Magnetic cantilevers and commercial MR sensors are employed. In section 4, a cantilever design custom-made for MR-SPM is presented, and micromagnetic simulations serve as the basis to estimate the achievable resolution. Section 5 concludes the paper.

2. Magnetoresistive sensors

Magnetoresistance is the property of a material to change the value of its electrical resistance when an external magnetic field is applied to it. Various physical phenomena can lead to magnetoresistance effects in a material. For example, giant magnetoresistance (GMR) structures use interface scattering of polarized conduction electrons as the mechanism for magnetoresistance. Two types of GMR structures are known, namely multilayer and spin-valve structures. GMR multilayers consist of alternate layers of ferromagnetic and nonferromagnetic conductors [35]. With a proper thickness of the nonmagnetic layer, there is an indirect exchange coupling between the magnetic layers, which magnetize adjacent magnetic layers in opposite directions in the absence of an applied magnetic field. This state is the higher resistance state. If a sufficiently large magnetic field is applied, the magnetic layers can be magnetized in the same direction, which is the lower resistance state. In a spin-valve structure, a thin conductor layer (normally copper) is sandwiched between two magnetic layers. One of them is a 'soft' ferromagnetic layer, which responds to the external magnetic field, and the other is a 'pinned' ferromagnetic layer, which does not. When the magnetizations in the two ferromagnetic layers are parallel, conduction electrons pass more freely between the magnetic layers than when the magnetizations are anti-parallel. Thus the resistance in the parallel magnetization case is lower than in the anti-parallel case. Pinning is usually accomplished by coupling of the pinned layer to an antiferromagnetic material through anti-parallel coupling [36].

MR sensors are typically used as magnetometers (gradiometers), read heads in hard disk drives, and random access memory (RAM) elements [35–38]. MR (spin-valve) sensors are also proposed for micro-electromechanical-system (MEMS) based sensor applications [39]. MR sensors can operate at very high bandwidth, as evidenced by their use as read heads and transducers in hard disk drives, whereas their use as RAM elements demonstrates their scaling potential. Moreover, they exhibit high sensitivity and low noise [40, 41]. MR sensors are characterized by their MR ratio, which is defined as the ratio of the maximum change in resistance when an external magnetic field is applied and the nominal resistance when no magnetic field is applied. GMR sensors have a particularly high MR ratio (for example, 110% in sputter-deposited Co/Cu multilayers [35]) and a wide range of operation.

From the discussion above, it is clear that MR sensors have very desirable characteristics, such as high bandwidth, small form factor and excellent scalability. Hence it would be advantageous to use MR sensors as integrated sensors for high-throughput SPM devices. The key challenge is the ability to translate the cantilever displacement into a substantial change in magnetic field as seen by a MR sensor. This aspect is addressed in this paper.

3. MR-SPM: principle of operation and experimental results

In this section, the concept of MR-SPM is demonstrated using experimental results. The essential idea of MR-SPM

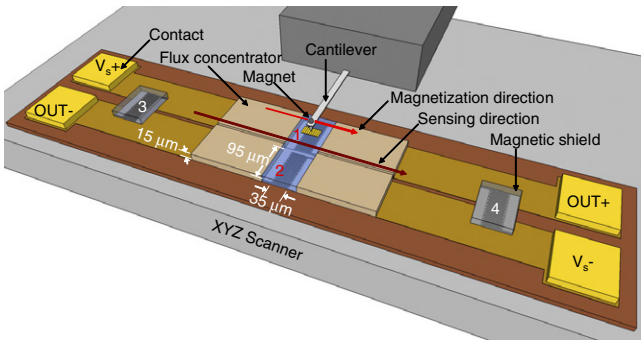

Figure 1. Schematic of the experimental setup to demonstrate MR-SPM.

is to translate the cantilever displacement into a change in the magnetic field as sensed by a MR sensor. One way to realize this is to translate the cantilever displacement into a change in the position of a micromagnet relative to a MR sensor. The micromagnet is attached to the distal end of the moving cantilever whereas the position of the MR sensor is fixed relative to the cantilever. An experiment was designed using magnetic cantilevers and commercial GMR sensors to demonstrate this scheme.

A schematic of the experimental setup is shown in figure 1. A FeNdBLa permanent magnetic particle was glued to the backside of a commercial cantilever above the tip using a heat-treatment adhesive [42]. The diameter of the micromagnet was approx. 10 μm and it was magnetized in the lateral direction, as shown in figure 1. The spring constant and the resonant frequency of the cantilever prior to gluing the magnetic particle were 0.1 N m^{-1} and 65 kHz, respectively.

A commercial multilayered GMR sensor chip in die form (NVE; AA005-01) was mounted on a nanopositioning stage with XYZ motion capability. One of the four sensing elements on this chip would serve as the sample, and patterns created on this element could be used for imaging purposes. Note that this configuration was employed only for the proof-of-concept experiment. For a cantilever custom-made for MR-SPM, it is better to place the MR sensor as described in section 4. The schematic of the GMR chip, drawn approximately to scale, is shown in figure 1. The four GMR elements are denoted by 1, 2, 3 and 4. They are connected in a Wheatstone bridge configuration to reduce noise. The GMR elements are approx. 95 μm long and 35 μm wide. The GMR elements 1 and 2 are exposed to the external magnetic field during measurement. The GMR elements saturate when the magnitude of the external magnetic field strength exceeds 100 Oe, whereas the linear range is between 10 and 70 Oe. The typical nominal resistance and the MR ratio of the GMR elements are 5 kΩ and 20%, respectively. The bandwidth of the commercial GMR sensor is specified to be larger than 1 MHz.

The cantilever with the micromagnet attached to it was fixed above GMR element 1 at a central position. Because of the small size of the micromagnet, it can be assumed that GMR element 2 was not affected by the stray magnetic field of the micromagnet. First an approach–retract curve was obtained using the cantilever and the sensor. The initial tip–sample separation was approx. 2.5 μm. The GMR chip was slowly raised by using the Z-scanner to approach the cantilever. This changed the position of the GMR sensing element relative to that of the fixed micromagnet, which in turn resulted in a change in the magnetic field sensed by the GMR element and hence its electrical resistance. The Z-scanner was moved up by approx. 2.75 μm and then retracted to its initial position. During the experiment, the resistance change of the GMR element was monitored using an electronic circuit. The resistance change as a function of the Z-scanner position is shown in figure 2(a). It can be seen that there is an almost linear change in the resistance as a function of the scanner position until the tip comes into contact with the sample. The sensitivity is given by the slope of this curve prior to the tip coming into contact with the sample and is 9.3 Ω μm^{-1}. Note that the topography of the sample will modulate the separation between the MR sensor and the micromagnet during imaging, which is captured by the off-contact signal. Ideally there would be no change in the resistance beyond the point of contact in the design shown in section 4. However, in this setup, further bending of the cantilever will cause a minor change in the resistance, which has little impact while performing contact-mode imaging at low loading force or during tapping-mode imaging, as will be demonstrated later.

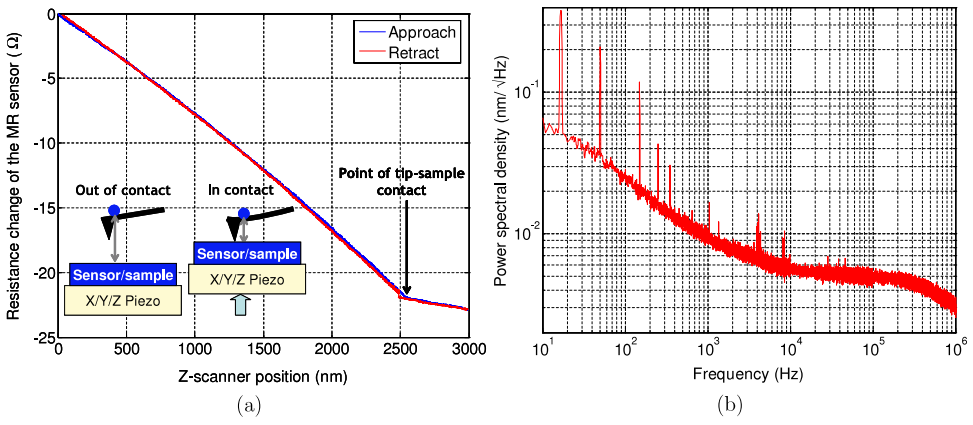

Figure 2. (a) An approach–retract curve obtained using the experimental setup. (b) Noise characteristic of the experimental setup.

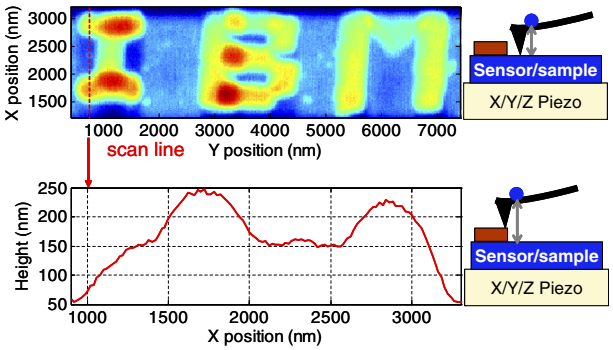

Figure 3. Top: constant-height, contact-mode image obtained using MR-SPM. Bottom: scan line across one amplitude profile.

The main sources of measurement noise in the GMR sensor are the electronic noise in the amplifiers, the intrinsic electromagnetic noise in the GMR elements, and the environmental electromagnetic noise in the setup. Following the approach–retract experiment, the magnetic cantilever was placed with its tip approx. 50 nm above the surface, and the noise signal from the GMR chip was captured. The noise spectrum of the SPM setup is shown in figure 2(b), where the previously calculated (out-of-contact) sensitivity value has been used to translate the measurement into nanometers. There is some $1/f$ noise, which predominates until approx. 10 kHz. However, beyond this frequency, the noise can be assumed to be white with a resolution of 5 pm $\mathrm{Hz}^{-1/2}$. Note that these commercial sensors can sense beyond a bandwidth of 1 MHz. The roll-off in the spectrum is due to the filters in the measurement circuit.

Contact-mode and tapping-mode imaging were performed with the MR-SPM setup to further illustrate the efficacy of the new sensing scheme. A platinum structure spelling 'IBM' was deposited on the GMR sensing element 1 using the focused ion beam (FIB) technique, so that it could be used for the imaging experiments. A contact-mode (constant-height) image of the sample surface obtained using the MR-SPM technique is shown in figure 3. As the tip traverses the sample topography, the relative position between the micromagnet and the GMR sensor is modulated. The measured height of the platinum structure (70–100 nm) is in accordance with the actual height of the fabricated structures.

Tapping-mode imaging is demonstrated next. The cantilever chip was mounted on a dither piezo. First, the frequency response of the cantilever was measured using an Agilent 4395A network analyzer. A 50 mV peak-to-peak chirp signal was generated by the analyzer and input to the dither piezo for acoustic actuation. The oscillation of the cantilever was measured by the GMR sensor chip. The deflection signal was fed back to the network analyzer, and the averaged frequency response data was collected. The frequency response is shown in figure 4(a). The first dominant resonant frequency and the quality factor of the cantilever are 11.84 kHz and 271.56, respectively. The rather low resonant frequency is due to the added mass of the glued-on micromagnet. The deflection signal from the GMR sensor was input to an analog lock-in amplifier (SR530 from Stanford Research Systems) and the demodulated amplitude and phase signals from the outputs were used for tapping-mode imaging. The sensitivity of the amplitude signal for sensing the topographical changes on the sample surface was measured in an approach-and-retract experiment. The amplitude of the freely oscillating cantilever was set to a constant value by applying a sinusoidal voltage signal of 11.8 kHz frequency to the dither piezo. An approach–retract curve was obtained in the same way as in the case of contact-mode operation. The Z-scanner was slowly moved towards the cantilever and then retracted to its initial position. The amplitude signal was calibrated by using the measured Z-scanner position. Subsequently, the amplitude of the input signal to the dither piezo was changed appropriately such that the amplitude of the freely oscillating cantilever was set to approx. 400 nm. The approach-and-retract experiment was repeated, and the corresponding experimental data is shown in figure 4(b). Note that the amplitude signal varies linearly with the position of the Z-scanner. Tapping-mode images of the sample surface were obtained in constant-height mode. The resulting image of the sample surface is shown in figure 5 (top). The amplitude profile for one scan line is shown in figure 5 (bottom). The amplitude signal is modulated by the sample profile as the tip traverses the sample surface. These results closely resemble those obtained in the contact-mode operation.

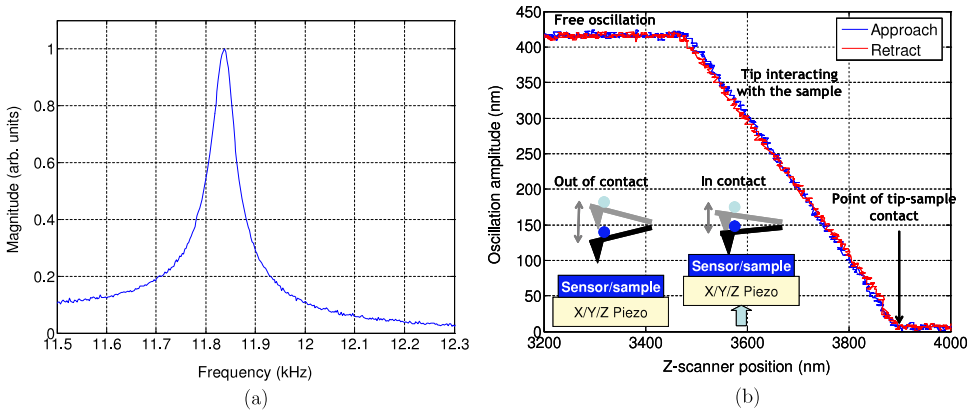

Figure 4. (a) Mechanical frequency response of the cantilever measured using the MR-sensing technique. (b) Approach–retract curve in tapping-mode.

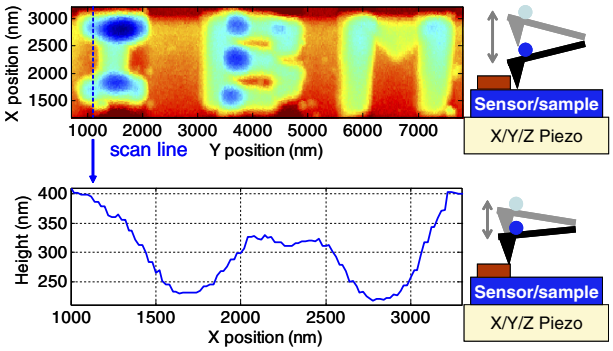

Figure 5. Top: constant-height, tapping-mode image obtained using MR-SPM. Bottom: scan line across one amplitude profile.

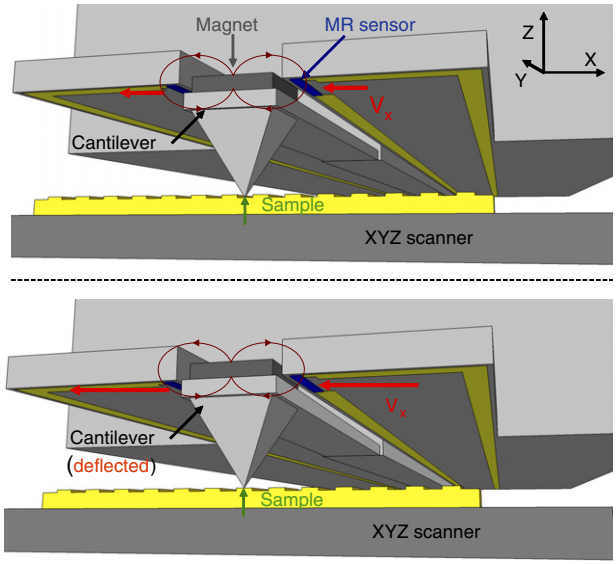

Figure 6. Schematic of a cantilever design custom-made for MR-SPM.

These experimental results demonstrate the concept of MR-SPM and the potential of this sensing scheme. It is truly remarkable that with a home-made magnetic cantilever and commercial GMR sensors one can perform regular AFM operations like contact-mode and tapping-mode imaging with very high resolution. Clearly, in these experiments, the relative orientation of the micromagnet and the MR sensor are not optimized to obtain maximum sensitivity. Also, the micromagnet is approximately ten times smaller than the available sensing area, which results in reduced sensitivity. In a custom-designed cantilever for MR-SPM these aspects can be addressed. In section 4, we describe one such cantilever design and evaluate the achievable resolution by means of micromagnetic simulations.

4. Cantilever design for MR-SPM

In this section, we introduce a cantilever custom designed for MR-SPM. The essential idea remains to translate the cantilever displacement into a change in the position of a micromagnet relative to a MR sensor. Unlike in the proof-of-concept experiment presented in section 3, the micromagnet and the MR sensors are now integrated on the same cantilever structure. The proposed cantilever design is henceforth referred to as the 'MR cantilever' and is schematically shown in figure 6. In the MR cantilever, a permanent micromagnet is fabricated at the flexible end on the backside of the cantilever just above the tip. A MEMS-compatible electroplating process can be used to fabricate such micromagnets. The MR sensors, which can be fabricated by sputtering, are deposited onto the bottom side of two rigid structures fabricated on either side of the moving part of the cantilever for easy electrical connection. The sensors are fabricated such that they are sensitive to the magnetic field component of the micromagnet along the width of the cantilever, i.e. the 'X'-axis in figure 6. The size and the position of the MR sensors and the permanent micromagnet are chosen such that the stray magnetic field strength, V_X, at the sensors remains small and the magnetic field gradient G of V_X along the vertical direction z, i.e., $G = \partial V_X/\partial z$ in Oe nm^{-1} is high. When the cantilever is at its unforced position, the average magnetic field strength at the MR sensor along the sensing direction is low. Depending upon the MR material, this may correspond to the maximal electrical resistance R of the sensor. When the cantilever experiences a tip–sample force and as a result deflects, the magnetic field passing through the MR sensor changes. If the probe deflects by z nm, then the magnetic field strength V_X at the sensor changes by Gz Oe. As a result, the resistance R of the MR sensor changes by $\Delta R = GzS$, where S is the MR sensitivity of the sensor in Ω Oe^{-1}. ΔR can be measured in constant-current or constant-voltage mode as a corresponding change in the voltage or the current, respectively, or it can also be measured by using an AC bias voltage. ΔR is the measure of the deflection of the cantilever. To sense the normal deflection of the cantilever with higher resolution, the two MR sensors may be used in summing mode. Alternatively, the two sensors may be used in differential mode to measure the torsion of the cantilever.

The sensitivity of MR-SPM can be assessed from micromagnetic simulations of the proposed micromagnet and MR sensor configuration shown in figure 6. For high sensitivity, a high magnetic field gradient, $\partial V_X/\partial z$, is required. Because the MR sensors usually have a small range of operation, also small magnetic field strength V_X is required. The shape, size, orientation and the relative positions of the micromagnet and the MR sensors dictate V_X and $\partial V_X/\partial z$ at the sensor. These parameters are calculated from micromagnetic simulations by using the 'object oriented micromagnetic framework' (OOMMF) [43] for the MR cantilever shown in figure 6.

For the MR cantilever, rectangular, cuboid-shaped micromagnets are considered because they are the simplest structure to fabricate by electroplating. The sensing direction of the MR sensor was fixed along the X-axis, and the magnetization direction of the micromagnet was fixed along the Z-axis. The cantilever deflection was also fixed along the Z-axis. The center of the micromagnet was fixed at the origin $(X, Y, Z) = (0, 0, 0)$. The saturation magnetization

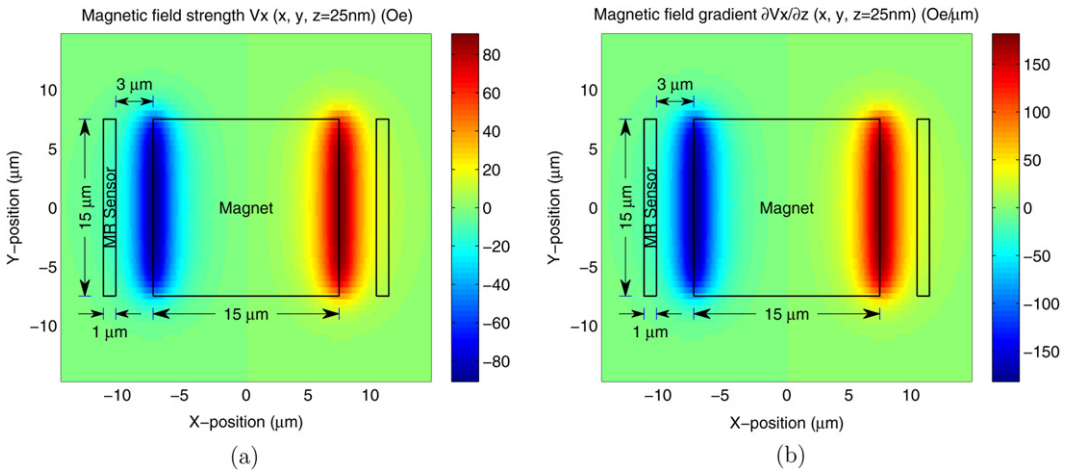

Figure 7. (a) Stray magnetic field strength and (b) gradient of the 15 μm × 15 μm × 3 μm large micromagnet.

of the magnetic material was set to 1.4×10^6 A m^{-1}. A uniform magnetic field of 1 T was applied along the Z-axis to magnetize the micromagnet.

Rectangular cuboid micromagnets of various sizes were considered in the simulations. The stray magnetic fields V of the micromagnets were analyzed over the three-dimensional space around the magnet to find a region in which the magnitude of the X-component of V, $|V_X|$, is low and the magnitude of the gradient of V_X along the Z-axis, $|\partial V_X/\partial z|$, is high. The minimum separation between the adjacent sides of the micromagnet and the MR sensor in the simulations is chosen to be 3 μm to ease the fabrication process.

Based on the simulation results, a rectangular cuboid micromagnet with length, depth and height of 15 μm, 15 μm and 3 μm, respectively, was chosen for the MR cantilever design. For this micromagnet, simulations showed that favorable conditions for $|V_X|$ and $|\partial V_X/\partial z|$ can be achieved in the XY-plane near $z = 0$. The distribution of V_X in the XY-plane at $z = 25$ nm is shown in figure 7(a). The Z-step size in the simulation was set to 50 nm, which generated grid points at −25 and 25 nm. Note that the stray magnetic field V of the micromagnet is distributed nonuniformly in the three-dimensional space around the micromagnet. In particular, V_X is distributed nonuniformly in the XY-plane at $Z = 25$ nm, as shown in figure 7(a). The magnitude of V_X is high near the micromagnet, and decreases in the XY-plane away from the micromagnet.

In this configuration, a MR sensor having a 1 μm × 15 μm size was chosen, positioned approx. 3 μm from the edge of the micromagnet. The average and maximum magnitude of V_X over the MR sensor were approx. 10.5 Oe and 15 Oe, respectively. It is essential that the magnitude of the magnetic field does not saturate the sensor. Most commercial MR sensors can comfortably operate in this regime. The distribution of the magnetic field gradient $\partial V_X/\partial z$ in the XY-plane at $z = 25$ nm is shown in figure 7(b). The average magnitude of the field gradient $|\partial V_X/\partial z|$ over the area of the MR sensor was approx. 22.64 Oe μm^{-1}. Note that larger MR sensors may be considered by compromising on $|\partial V_X/\partial z|$.

The resolution of the MR cantilever can be estimated by using the magnetic field gradient and the magnetic field resolution of the MR sensors. For typical commercial MR sensors, the resolvable magnetic field typically varies between 0.15 and 1.5 nT Hz$^{-1/2}$ [40]. For our calculations we chose the resolution figures associated with GMR sensors from NVE Corporation, which is $\text{Res}_{\text{GMR}} \approx 0.27$ nT Hz$^{-1/2}$ $= 2.7 \times 10^{-6}$ Oe Hz$^{-1/2}$.

From the micromagnetic simulations, we had obtained an average value of the magnitude of the magnetic field gradient at the sensors, $|\partial V_X/\partial z|_{\text{ave}}$, of 22.64 Oe μm^{-1}. Hence, the resolution of the MR-sensor-based deflection sensing technique using one sensor is estimated as $1/|\partial V_X/\partial z|_{\text{ave}} \times \text{Res}_{\text{GMR}} = 1/22.64 \times 2.7 \times 10^{-6}$ μm Hz$^{-1/2}$ $\approx 1.19 \times 10^{-4}$ nm Hz$^{-1/2}$. Because two MR sensors are employed in the MR cantilever in figure 6, the resolution is further improved by a factor of $\sqrt{2}$ to 8.43×10^{-5} nm Hz$^{-1/2}$. Assuming a white noise level of 8.43×10^{-5} nm Hz$^{-1/2}$, a resolution of 84 pm can be achieved over a bandwidth of 1 MHz. This is a truly remarkable number given that the achievable resolution using optical means in state-of-the-art AFMs exceeds 200 pm over the same bandwidth. Further optimization of the cantilever geometry and the selection of more advanced MR sensors, such as tunnel magnetoresistive (TMR) sensors, can lead to even better resolution. Because the torsion of the cantilever is measured by operating the two MR sensors in differential mode, the resolution of torsion measurement is $\sqrt{2}$ times worse than the resolution of a single MR sensor.

5. Conclusions

MR-sensor-based cantilever displacement sensing is a new paradigm for SPM that promises high resolution at very high bandwidth, enabling high-speed and high-throughput operation. The key idea in MR-SPM is to translate the cantilever displacement into a relative motion between a micromagnet and a MR sensor. Thus the displacement signal is translated into a magnetic field change as seen by the MR sensor. The electrical resistance of the MR sensor is a function of the magnetic field, and hence the deflection signal can

be measured as a resistance signal. The concept of MR-SPM is demonstrated experimentally using commercial GMR sensors and magnetic cantilevers. A spherical micromagnet is glued onto the cantilever, and the MR sensor, which also serves as the sample, is used to sense its deflection. Images of a platinum micro-structure with a nominal height of 70 nm were obtained in both contact-mode and tapping-mode operation. A custom-made MR cantilever design with an integrated micromagnet and MR sensors is presented that can be used for SPM applications. Micromagnetic simulations are performed to estimate the resolution of the sensing scheme using such a cantilever. The resolution is estimated to be a remarkable 84 pm over a 1 MHz bandwidth. MR-SPM has the potential to address the need for high-bandwidth, high-resolution integrated sensing. SPM-based devices employing several MR cantilevers for high throughput and large field-of-view can be manufactured. At the same time, MR cantilevers can also be employed to realize compact and low-cost scanning probe microscopes, as alternatives to the current AFMs, which employ bulky and costly optical deflection sensing means.

Acknowledgments

We would like to acknowledge the contributions of several colleagues at IBM Research—Zurich, in particular Mark Lantz for providing the magnetic microcantilevers and Peter Bächtold for the electronic setup. We would also like to thank our colleagues Gian Salis, Michel Despont, Urs Dürig and Armin W Knoll for stimulating discussions.

References

[1] Carrascosa L G, Moreno M, Álvarez M and Lechuga L M 2006 Nanomechanical biosensors: a new sensing tool *Trends Anal. Chem.* **25** 196–206
[2] Oliver R A 2008 Advances in AFM for the electrical characterization of semiconductors *Rep. Prog. Phys.* **71** 076501
[3] Pires D *et al* 2010 Nanoscale three-dimensional patterning of molecular resists by scanning probes *Science* **328** 732–5
[4] Knoll A W *et al* 2010 Probe-based 3D nanolithography using self-amplified depolymerization polymers *Adv. Mater.* **22** 3361–5
[5] Wei Z *et al* 2010 Nanoscale tunable reduction of graphene oxide for graphene electronics *Science* **328** 1373–6
[6] Pantazi A *et al* 2008 Probe-based ultrahigh-density storage technology *IBM J. Res. Dev.* **52** 493–511
[7] Rangelow I W *et al* 2007 Piezoresistive and self-actuated 128-cantilever arrays for nanotechnology applications *Microelectron. Eng.* **84** 1260–4
[8] Minne S C 1998 Automated parallel high-speed atomic force microscopy *Appl. Phys. Lett.* **72** 2340–2
[9] Manalis S R, Minne S C, Quate C F, Yaralioglu G G and Atalar A 1997 Sequential position readout from arrays of micromechanical cantilever sensors *Appl. Phys. Lett.* **70** 3311–3
[10] Miller S A, Turner K L and MacDonald N C 1997 Microelectromechanical scanning probe instruments for array architectures *Rev. Sci. Instrum.* **68** 4155–62
[11] Lang H P *et al* 1998 A chemical sensor based on a micromechanical cantilever array for the identification of gases and vapors *Appl. Phys.* A **66** S61–4
[12] Ando T, Kodera N, Takai E, Maruyama D, Saito K and Toda A 2001 A high-speed atomic force microscope for studying biological macromolecules *Proc. Natl Acad. Sci. USA* **98** 12468–72
[13] Humphris A D L, Miles M J and Hobbs J K 2005 A mechanical microscope: high-speed atomic force microscopy *Appl. Phys. Lett.* **86** 034106
[14] Fantner G E *et al* 2006 Components for high speed atomic force microscopy *Ultramicroscopy* **106** 881–7
[15] Takeshi F 2009 Wideband low-noise optical beam deflection sensor with photothermal excitation for liquid-environment atomic force microscopy *Rev. Sci. Instrum.* **80** 023707
[16] Fritz J *et al* 2000 Translating biomolecular recognition into nanomechanics *Science* **288** 316–8
[17] Álvarez M and Tamayo J 2005 Optical sequential readout of microcantilever arrays for biological detection *Sensors Actuators* B **106** 687–90
[18] Yue M *et al* 2004 A 2D microcantilever array for multiplexed biomolecular analysis *J. Microelectromech. Syst.* **13** 290–9
[19] Sulchek T *et al* 2001 Parallel atomic force microscopy with optical interferometric detection *Appl. Phys. Lett.* **78** 1787–9
[20] Kocabas C and Aydinli A 2005 Design and analysis of an integrated optical sensor for scanning force microscopies *IEEE Sensors J.* **5** 411–8
[21] Burcham K E, Brabander G N D and Boyd J T 1992 Micromachined silicon cantilever beam accelerometer incorporating an integrated optical waveguide *Proc. SPIE* **1793** 12–8
[22] Wu S and Frankena H J 1992 Integrated optical sensors using micromechanical bridges and cantilevers *Proc. SPIE* **1793** 83–9
[23] Zinoviev K, Dominguez C, Plaza J A, Busto V J C and Lechuga L M 2006 A novel optical waveguide microcantilever sensor for the detection of nanomechanical forces *J. Lightwave Technol.* **24** 377–82
[24] Nordströrm M, Zauner D A, Calleja M, Hübner J and Boisen A 2007 Integrated optical readout for miniaturization of cantilever-based sensor system *Appl. Phys. Lett.* **91** 103512
[25] Li M, Pernice W H P and Tang H X 2009 Broadband all-photonic transduction of nanocantilevers *Nat. Nanotechnol.* **4** 377–82
[26] Hu W *et al* 2009 Demonstration of microcantilever array with simultaneous readout using an in-plane photonic transduction method *Rev. Sci. Instrum.* **80** 085101
[27] Tortonese M, Barrett R C and Quate C F 1993 Atomic resolution with an atomic force microscope using piezoresistive detection *Appl. Phys. Lett.* **62** 834–6
[28] Indermühle P F, Schürmann G A and Rooij N F 1997 Fabrication and characterization of cantilevers with integrated sharp tips and piezoelectric elements for actuation and detection for parallel AFM applications *Sensors Actuators* A **60** 186–90
[29] Hansen O and Boisen A 1999 Atomic resolution with an atomic force microscope using piezoresistive detection *Nanotechnolgy* **10** 51–60
[30] Neubauer G, Cohen S R, McClelland G M, Horn D E and Mate C M 1990 Force microscopy with a bidirectional capacitance sensor *Rev. Sci. Instrum.* **61** 2296–308
[31] Sebastian A and Wiesmann D 2008 Modeling and experimental identification of silicon microheater dynamics: a systems approach *J. Microelectromech. Syst.* **17** 911–20
[32] Nakamura M, Kimura M, Sueoka K and Mukasa K 2002 Scanning magnetoresistance microscopy with a magnetoresistive sensor cantilever *Appl. Phys. Lett.* **80** 2713–5
[33] Takezaki T, Yagisawa D and Sueoka K 2006 Magnetic field measurement using scanning magnetoresistance microscope with spin-valve sensor *Japan. J. Appl. Phys.* **45** 2251–4

[34] Sahoo D R, Sebastian A, Häberle W, Pozidis H and Eleftheriou E 2009 Magnetoresistive sensor based scanning probe microscopy *Proc. 9th IEEE Nanotech. Conf.* pp 862–5
[35] Parkin S S P, Jiang X, Kaiser C, Panchula A, Roche K and Samant M 2003 Magnetically engineered spintronic sensors and memory *Proc. IEEE* **91** 661–80
[36] Daughton J 2003 Spin-dependent sensors *Proc. IEEE* **91** 681–6
[37] Katti R R 2003 Giant magnetoresistive random-access memories based on current-in-plane devices *Proc. IEEE* **91** 687–702
[38] Tehrani S *et al* 2003 Magnetoresistive random access memory using magnetic tunnel junctions *Proc. IEEE* **91** 703–14
[39] Li H, Boucinha M, Freitas P P, Gaspar J, Chu V and Conde J P 2002 Microelectromechanical system microbridge deflection monitoring using integrated spin valve sensors and micromagnets *J. Appl. Phys.* **91** 7774–6
[40] Stutzke N A, Russek S E, Pappas D P and Tondra M 2005 Low-frequency noise measurements on commercial magnetoresistive magnetic field sensors *J. Appl. Phys.* **97** 10Q107
[41] Ramírez D, Pelegrí J, Navarro A E and Casans S 2000 Characterization of giant magnetoresistance effect based sensors and its applications *Proc. 17th IEEE Instrum. Meas. Conf.* vol 2, p 571
[42] Lantz M A, Jarvis S P and Tokumoto H 2001 High resolution eddy current microscopy *Appl. Phys. Lett.* **78** 383–5
[43] The Object Oriented MicroMagnetic Framework (OOMMF) project at Information Technology Laboratory, National Institute of Standards and Technology, USA http://math.nist.gov/oommf/